LAWRENCE
LIVERMORE
NATIONAL
LABORATORY

LLNL-CONF-636484

EVALUATION OF A GEOTHERMAL PROSPECT USING A STOCHASTIC JOINT INVERSION MODELING PROCEDURE

A. Tompson, R. Mellors, A. Ramirez, M. Chen, K. Dyer, X. Yang, J. Wagoner, W. Trainor-Guitton

May 13, 2013

Geothermal Resources Council Annual Meeting
Las Vegas, NV, United States
September 29, 2013 through October 2, 2013

Disclaimer

EVALUATION OF A GEOTHERMAL PROSPECT USING A STOCHASTIC JOINT INVERSION MODELING PROCEDURE

A. F. B. Tompson, R. J. Mellors, A. Ramirez, M. Chen, K. Dyer, X. Yang, J. Wagoner, and W. Trainor-Guitton

Lawrence Livermore National Laboratory, 7000 East Avenue, Livermore, CA, 94550, USA
Email: tompson1@llnl.gov

ABSTRACT

A stochastic inverse algorithm to jointly analyze multiple geophysical and hydrological datasets for a geothermal prospect is presented. The purpose is to improve prospect evaluation and estimate the likelihood of useful temperature and fluid flow fields at depth. The approach combines Bayesian inference with a Markov Chain Monte Carlo (MCMC) global search algorithm to conduct a staged, model-based inversion of the different data sets. Initial estimates of uncertainty in structural or parametric characteristics of the prospect are used to drive large numbers of simulations of hydrothermal fluid flow and related geophysical processes using random realizations of the conceptual geothermal system. The results consist of a subset of these realizations – an equally probable ensemble of alternatives – that best match the observed datasets within a specified norm or tolerance. Statistical (posterior) characteristics of these solutions reflect reductions in the perceived (prior) uncertainties. The method is highly flexible and capable of accommodating multiple and diverse datasets as a means to maximize the utility of all available data to understand system behavior.

INTRODUCTION

The primary objective of geothermal exploration is to find and characterize commercial sources of geothermal energy. Favorable geothermal prospects require sufficient quantities of heat and groundwater, as well as adequate (hydraulic) permeability to support groundwater circulation. As these elements can be difficult to resolve or fully characterize in the subsurface, geothermal exploration usually employs multiple geophysical, hydrologic, and geochemical methods to describe a geothermal system as much as possible, often prior to any significant drilling efforts. Although such characterization efforts often utilize predictive numerical models to describe the temperature and fluid flow distributions in the subsurface, the models are typically subject to uncertainty in structural or parametric characteristics of the system, which can limit the quality of interpretations that can be made with their results. Ideally, models constructed for geothermal exploration will seek to include contributions from, and, in the end, be consistent with all forms of characterization data available.

This paper outlines a joint inversion methodology to utilize multiple geophysical, thermal, and hydrological data sets in the construction of such a numerical model. Recognizing the inherent uncertainties in structural, parametric, and other characteristics of subsurface systems, the approach uses stochastic representations of uncertain variables or structural features (with prior distributions) to drive a generalized Markov Chain Monte Carlo (MCMC) inversion procedure. This process will yield a distribution of plausible or "accepted" results rather than one single answer, each of which is quantitatively consistent with observations to within a specified degree of error or tolerance. The range or (posterior) distribution of uncertain variables or structural

features in the "accepted" results will be reduced, indicating measured reductions of uncertainty in the stochastic variables, improving the quantitative evaluation of the prospect. The algorithm possesses several advantages:

- It is extremely flexible in terms of the geothermal systems it can be used for and the data that it can incorporate;
- It searches the global solution space defined by the stochastic variable distributions; and
- It provides robust estimates of uncertainty and its reduction.

The current procedure is based on a similar one used in Ramirez et al., (2005; 2012). Other studies with similar approaches applied to geothermal prospects include Jardani and Revil (2009) and Chen et al. (2012).

EXAMPLE APPLICATION

As a means to better describe the inversion approach, a series of initial simplified applications to a geothermal prospect located in the western Salton Trough in California will be considered. The site is adjacent to Superstition Mountain (Figures 1, 2) in Imperial County and is currently under investigation by the Navy geothermal program (e.g. Bjornstad et al., 2006; Tiedeman et al., 2011). Readily available geological and geophysical data include three thermal gradient exploration boreholes, borehole resistivity logs, magnetotelluric and gravity geophysical surveys, surface heat flux measurements, and other nearby hydrologic and geologic data tabulated or referred to in Tompson et al. (2008). A principal aim of the initial application is to evaluate algorithm performance, parametric sensitivities, and broader feasibility with respect to increasing complexity of the model system. A significant question is how and in what ways this type of inversion can be best applied and interpreted since it is computationally expensive, requiring thousands of "forward" simulations.

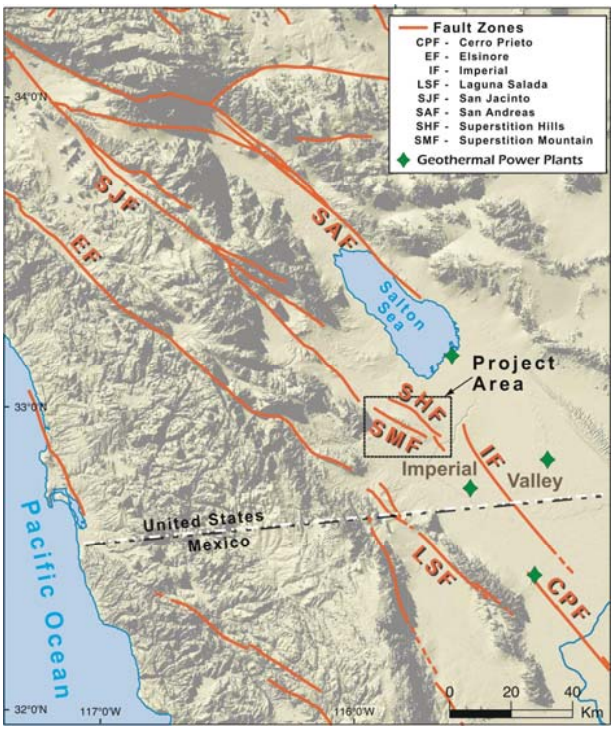

Figure 1: Location of the Superstition mountain project area in Imperial County, CA (Bjornstad et al., 2006*)*

The first step in the application will involve the development of a provisional hydrothermal groundwater flow model to match the temperature observations in the three exploration boreholes. Subsequent steps may seek to refine the model further to be consistent with geophysical surveys, heat flux data, or even geochemistry observations.

The locations of the boreholes relative to Superstition Mountain and nearby faults and faulted areas are shown in Figure 2. Boreholes NAFEC-1, NAFEC-2, and NAFEC-3 were drilled to depths of 695 m (2,280 ft.), 652 m (2,140 ft.), and 1,067 m (3,500 ft.), respectively. As close as the boreholes are to one another, their temperature profiles show distinctly different

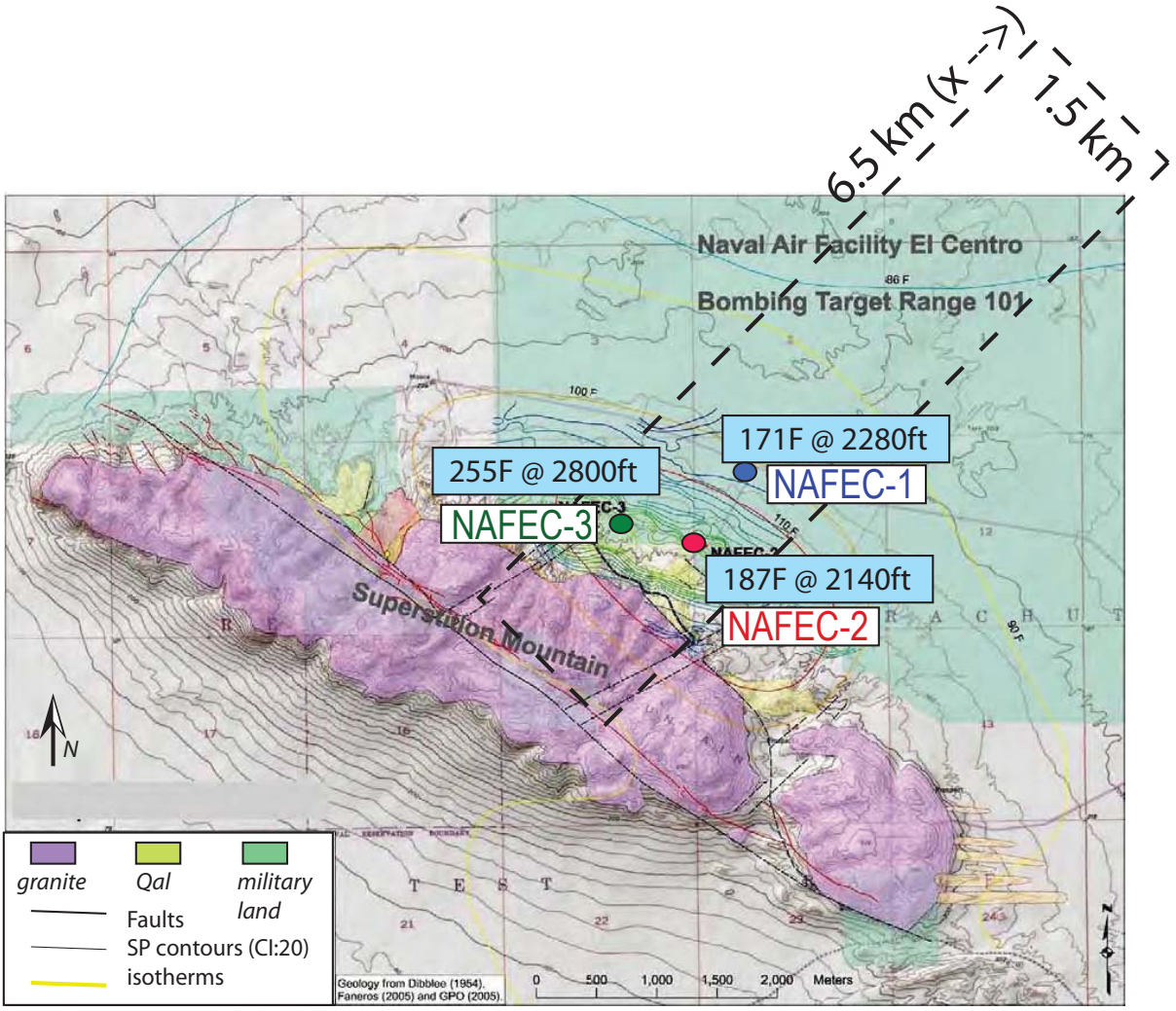

Figure 2: Geologic map of prospect (bottom) showing surface geology and geophysical measurements with temperature profiles of the three test wells (Figure 3). Dashed lines show the areal projection of the bounded modeling domain used in the application of the hydrothermal flow and resistivity models. Adapted from Tiedeman et al., (2011).

behavior (Figure 3). The thermal profile in NAFEC-3 is the warmest of all three (124°C at 853 m, or 255°F at 2,800 ft.) and reaches its highest temperature at a depth above its bottom. The slight cooling observed below this depth suggests a buoyancy-driven flow or recirculation of groundwater. The profile above the 122 m (400 ft.) depth shows a noticeable break or transition to a linear, conduction-dominated profile, indicative of little or no flow of groundwater. The thermal profile in NAFEC-1 is the coolest of the three, and exhibits a linear, or conduction dominated profile throughout its entire depth, reaching its maximum temperature at its bottom (77°C at 695 m, or 171°F at 2,280 ft.). This suggests that little or no buoyancy-driven groundwater flow is occurring anywhere along its depth. At NAFEC-2, an intermediate profile is evident, revealing linear behavior above the 122 m (400 ft.) depth (as in the others), linear behavior below 244 m (800 ft.) depth (reaching a maximum value of 86°C at 652 m, or 187°F at 2,140 ft.), and a transition zone in-between suggestive of some recirculating flows over this thin (122 m, or 400 ft.) horizon.

The observed breaks in temperature profiles above the 122 m (400 ft.) depth would appear to be due to the position of an impermeable layer or the local water table, either of which would inhibit higher groundwater circulation effects. The latter possibility is consistent with regional water table interpretations (Dutcher et al., 1972, Fig. 13) and resistivity logs in the wells. When viewed in Figure 2, the areal variations in borehole temperatures seem to suggest a localized type of enhanced geothermal activity or circulation evident in the immediate vicinity of NAFEC-2 and NAFEC-3. Shallower borehole temperature profiles (~ 61 m, or 200 ft. depth) shown in this figure are also indicative of a confined geothermal influence, again, chiefly in the vicinity of NAFEC-2 and NAFEC-3.

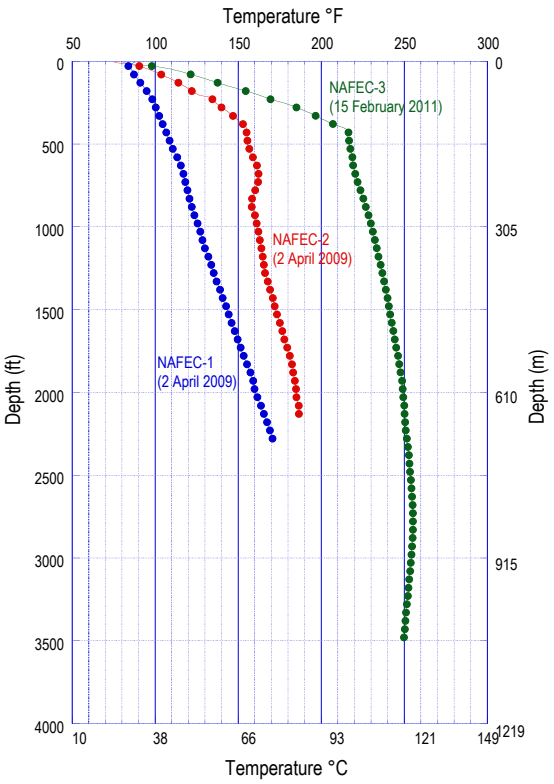

Figure 3: Temperature profiles in the three "NAFEC" wells. Adapted from Tiedeman et al., (2011).

An initial 3-D geologic model is used as a starting basis for building the provisional hydrothermal groundwater flow model. The geologic model is based on analyses of previous work near Superstition Mountain (e.g., Dutcher et al., 1972; Loeltz, et al., 1975; Bjornstad et al., 2006; Tiedeman et al., 2011, Tompson et al, 2008, as described further below). Uncertain material properties such as permeability, porosity, and heat capacity are allowed to vary in the hydrothermal simulation model, as well as certain structural features of the geologic model such as the extent and properties of a postulated fault zone.

INVERSION APPROACH

The proposed stochastic inversion approach combines Bayesian inference with a MCMC global search algorithm to conduct a staged, model-based inversion of different available data sets, based on the method proposed by Mosegaard and Tarantola, (1995). For a given stage, the inversion process selects models that are consistent with available data. Joint inversion is accomplished by cascading sequential model-based stages, one for each type of data set. Moving from one inversion stage to the next is only pursued if the model in the first stage is "accepted" or deemed consistent with the observed data for that stage. In this way, models that emerge from the final stage will be consistent with all data. Figure 4 illustrates the application of a two-stage MCMC process to the example problem where both the NAFEC well temperature data and a set of electrical resistivity data are available. Additional sets of geophysical data, such as magneto-telluric, gravity or heat flux observations will be considered in the future.

In the first stage of the process, a 3-D hydrothermal flow model is used to predict equilibrium (steady state) temperature and fluid flow fields for a sequence of random model configurations (realizations) drawn from the uncertain (prior) parameter distributions. Each "forward" solution is developed from a common set of pressure and thermal boundary conditions and is compared with the observed temperature data. The likelihood that a given realization reproduces the

observed temperature data is calculated from the fit of the calculated data to the actual observations. The fit is calculated using a vector error norm (including estimated measurement errors) accrued across the field or space of data where comparisons can be made. If the likelihood is sufficiently high, then that particular realization is "accepted" and considered for a subsequent Stage 2 calculation; otherwise, it is rejected, and another Stage 1 realization is considered.

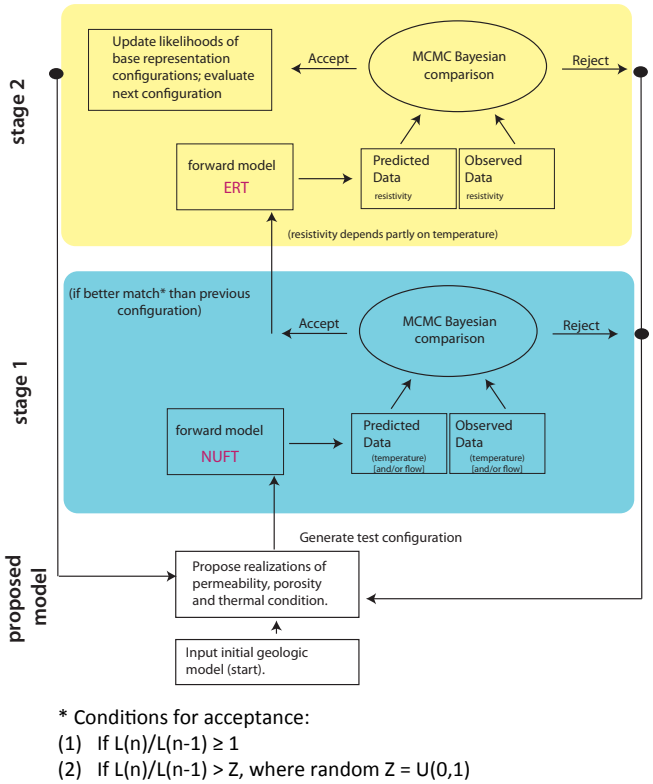

* Conditions for acceptance:
(1) If L(n)/L(n-1) ≥ 1
(2) If L(n)/L(n-1) > Z, where random Z = U(0,1)

Figure 4: Schematic diagram of the two-stage inversion method. An initial geologic model with hydrologic and thermal constraints is selected (bottom). In stage one, it is run until equilibrium using NUFT and the simulated well temperatures are compared with observations. In stage two, assuming stage one acceptance, the expected resistivity of the model is calculated and then compared with the data. The final output is a ranked set of models and associated probabilities.

In the second stage of the process, electrical resistivity distributions for the "accepted" realizations of Stage 1 are simulated and compared to the resistivity observations using an analogous likelihood calculation. "Accepted" results from Stage 2 populate a (posterior) distribution of models that are consistent with both sets of data. This cycle is repeated over a sufficient number of realizations until the posterior distribution converges to a stable solution. The procedure is guaranteed to converge to a unique, invariant limiting distribution from any starting trial model, provided that there are sufficient steps (trials) in the Markov chain.

The decision to accept or reject a particular model realization in a data comparison step is a probabilistic process (Metropolis et. al., 1953). A proposed model – call it realization n – is always accepted if its likelihood, L(n), is greater than the that of the previous realization L(n-1). Alternatively, if L(n) < L(n-1), the probability of acceptance is L(n)/L(n-1). The second condition is included to allow the global search process to avoid local maxima.

In the sequence of Monte Carlo realizations, each new simulation is drawn from statistical distributions of the uncertain parameters or variables. For example, the permeability is sampled from log uniform distributions in each geologic unit and is correlated with porosity. The bulk thermal conductivity of the formation as a whole is controlled by the intrinsic thermal

conductivities of the rock and water and by the saturated porosity. The bulk electrical resistivity of the formation is a function of its temperature, degree of saturation, and the intrinsic resistivity of rock and groundwater, the latter of which is heavily influenced by its salinity. Although fluid salinity is held fixed in the present implementation, it may become a powerful constraint in future steps owing to significant salinity contrasts in the basin groundwater (Tompson et al., 2008).

The stochastic inversion framework is written in Python and incorporates various compiled forward codes for each modeled step of the process. We have adapted hydrothermal fluid flow and DC resistivity models into the current version of the framework and will add others as the project matures. Fluid and heat flow are simulated using NUFT (Nonisothermal, Unsaturated Flow and Transport), a 3-D multi-phase hydrothermal flow and transport model based upon an integrated finite difference discretization (Nitao, 1998, 2000). Electrical resistivity is simulated using Multibh, a 3-D finite difference forward modeling code that predicts electrical resistance for arbitrary electrode configurations and electrical resistivity models (LaBrecque et al., 1999). We recognize that DC resistivity is not commonly used in geothermal exploration but the code was readily available and we are essentially using it as a placeholder in the inversion framework for a magneto-telluric (MT) code whose development is in progress.

The flexibility of the algorithm makes adding additional forward modeling codes straightforward, although use of different grid or meshing schemes in the underlying suite of models can add complications.

PROVISIONAL HYDROTHERMAL MODEL

Geologic Structure: A three-dimensional geologic model of the Salton Sea Basin was developed in Tompson et al. (2008) and is being used to further conceptualize the geologic structure underneath Superstition Mountain. This model was built with the Earth Vision software product and uses digital elevation model (DEM) data from the US and Mexico, several externally provided models of the basin architecture, other known tectonic features, and related geologic interpretations (e.g., Dutcher et al., 1972; Loeltz, et al., 1975; Bjornstad et al., 2006; Tiedeman et al., 2011). Additional interpretations available in the vicinity of Superstition Mountain have been used with geophysical and drilling logs from the three NAFEC boreholes to refine the model (Figure 5). This approach easily facilitates a volumetric analysis of the geologic units shown in (Table 1) which range vertically from the ground surface (or surface topography) past the bottom of the Imperial formation into the granitic basement rock. Figure 5 clearly shows Superstition Mountain as a surficial manifestation of the older granitic bedrock, bounded by faults and more recent marine and alluvial sedimentary rock draping off to either side. The location and depths of the NAFEC wells are also shown.

Faults and Hypothesized Fluid Pathways: Examination of the known and perceived faults near Superstition Mountain (chiefly, the Superstition Mountain Fault and related cross-oriented features, e.g., as shown in Figure 2), recent earthquake data in the vicinity (e.g., Tiedman et al 2011), and surface observations of calcite veining and hydrothermal mineral alteration (Layman Energy Associates, 2012) support a hypothesis that localized zones of enhanced permeability along one of more of the preliminary principal or cross-oriented faulted areas facilitate the vertical invasion of hot geothermal fluids from deeper zones (> 3000 ft.) into shallower depths (< 1000 ft.). This circulation is believed to become manifest in the elevated temperatures observed in the NAFEC boreholes and in nearby shallow borehole temperature surveys.

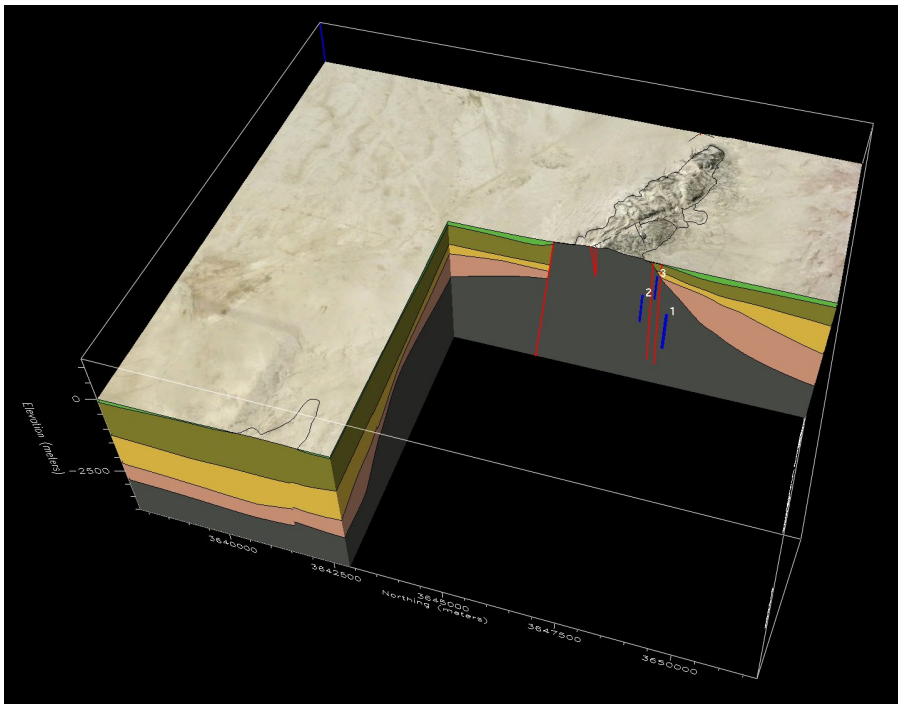

Figure 5: Geologic model in the vicinity of Superstition Mountain, looking from the East (foreground) to the West, and showing (from bottom) the granitic basement and the Imperial, Borrego/Palm Springs, Brawley, and Post Brawley formations (Table 1). Faulted areas shown in red; projected locations of the NAFEC wells shown in blue. Elevations indicated in meters above seal level.

Provisional Flow Model Domain: Figure 2 shows a provisional bounded domain that is being considered for the preliminary application of the hydrothermal groundwater model. The domain is parallel with the NW-SW orientation of Superstition Mountain and primary fault directions and has been made to extend 6.5 km to the northeast and to a depth of 3.2 km. The smaller 1.5 km width was chosen to accommodate the earliest calibration and inversion testing exercises, but will be expanded later to support larger areas and more mature inversion tests. The domain has been chosen to incorporate the three NAFEC wells, with NAFEC-3 lying close to the mountain and in a zone of perceived, cross-oriented faulting, NAFEC-1 lying furthest from the mountain, away from any perceived faulting, and NAFEC-2, in between, in both respects. As shown in plan view, the domain is 6.5 km long (in the local x-coordinate direction) by 1.5 km wide (in the local y-direction), and it extends 3.2 km below the ground surface (in the local z-direction). The discretization of this domain is based upon 100 m cubic grid blocks as shown in Figure 6.

For simplicity, the preliminary model has adopted several simplifying assumptions in terms of the representation of the geologic model and the physical processes considered (Figure 6). These include:

- An approximate representation of the faulted (granitic) basement and Imperial (sandstone), Borrego / Palm Springs (sandstone and delta sediments), Brawley (sandy sediments) and Post Brawley (lacustrine sediments and clay) formations across the model cross section;
- Two 100-m thick planar faulted zones, one (A) occupying the entire SW face of the domain at x = 0, consistent with the Superstition Mountain Fault (SMF), and another (B) a hypothesized vertical conjugate fault (CF), transverse to and extending away from (A) to the NE, of uncertain length and height, that potentially facilitates hydrothermal flow from depth;

- Specification of a slight downward slope of the top of the model from the SW to the NE, consistent with the local topography;
- Specification of saturated conditions throughout the entire model depth (for now), which will be adjusted later to reflect an apparent water table at a depth between 100 and 120 m (~350 and 400 ft.; Dutcher et al., 1972);
- Specification of fixed temperatures of 27° and 150°C at the top and bottom of the domain (~80° and 300°F respectively); and
- Specification of hydrostatic pressures at the SW and NE ends of the model, leading to a slight, imposed hydraulic gradient to the NE.

Table 1: Geologic units and associated permeabilities included in provisional hydrothermal model; Random values for Ti and CF units in MCMC runs based upon a log-uniform distribution as shown, $\log_{10}(k) = \langle \log_{10}(k) \rangle + Z$ where $Z \sim U(-.173, +.173)$, $\langle Z \rangle = 0$, and $\sigma_z = 0.1$.

Unit (name and code)		Materials	Permeability, k (m^2)	Prior pdf for k
Atmosphere		air	1.00E-08	
Post Brawley Formation	Qb	low permeability lacustrine, delta sediments, clays	2.00E-15	
Brawley Formation	Tp1	sandy sediments	2.00E-14	
Borrego / Palm Springs Formation	Tp2	low permeability sandstone, delta sediments	4.00E-15	
Imperial Formation	Ti	high permeability sandstone	Random	$\text{Log}_{10}(k) \sim -14 + Z$
Basement	Granite	granitic rock	1.00E-18	
Superstition Mountain Fault (A)	SMF	more permeable granitic rock	1.00E-13	
Conjugate Fault (B)	CF	more permeable granitic rock	Random	$\text{Log}_{10}(k) \sim -13 + Z$

Within this conceptualization, zones of higher permeability occur within certain layers (Figure 6, yellow) – the more sandy sediments, for example – and within the faults (Figure 6 dark blue or pink). Choices for permeability magnitudes and their statistical distributions were motivated by discussions in Tompson et al (2008) and references therein. The geometry of the hypothesized fault (B) is based on other conjugate faults in the immediate region, such as the Superstition Hill/Elmore Ranch faults a few km to the east.

Mesh Design and Parameterization Considerations: Mesh design is a challenge for several reasons. First, there are the customary balances between minimizing computational cost while maintaining adequate spatial resolution, particularly within an MCMC simulation framework.

Second, different models in different stages of the MCMC framework need to share data, yet may have different meshing requirements. For example, although the hydrothermal flow and resistivity models share the same core mesh (100-m cubic grid, Figure 6), the resistivity mesh must have an extended portion reaching into the far field for boundary condition specification, making it much larger than the hydrothermal flow model domain.

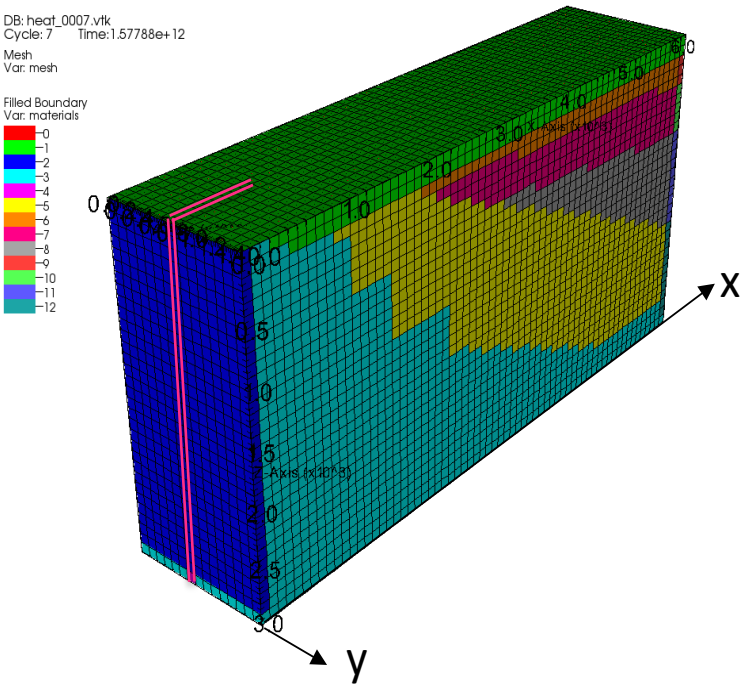

Figure 6: Provisional simulation grid for the provisional groundwater flow model, showing, in color, fields associated with geologic units and faulted areas. Superstition Mountain Fault is in the foreground. Pink lines show projected location of embedded conjugate fault. The simulation is 6.5 km long, 1.5 km wide, and 3.2 km deep, with fixed 100-m cube grid blocks.

Within the core modeling mesh (Figure 6), both the hydrothermal flow and resistivity models share the same 100-m cubic grid. Each grid cell is assigned to a particular formation material or unit (such as granite) to which model-related properties (e.g., permeability, porosity, and heat capacity) are assigned in each realization simulation. For the MCMC processes considered in the inversion scenarios below, some of the material properties are drawn from a (prior) probability distribution during each realization simulation while others are held fixed (Table 1). In addition, several dimensional characteristics of the CF fault (B) are also chosen from (prior) uniformly random distributions. This fault is assumed to be anchored at the SMF fault (A) at location x = 0 and extend a random distance into the domain (positive x-direction). It is also assumed to be anchored at the bottom of the domain and extend a random distance vertically upward into the domain. In some cases, its width and registration along the y-axis may also be considered random. These "structural" features are accommodated by re-assigning material "fault" properties for the set of cells that comprise the fault geometry drawn in each realization.

INVERSION SCENARIOS

Two inversion test scenarios were developed for initial evaluation of the method. In the first (**Scenario 1**), a synthetic (control) dataset was generated from an arbitrary, random realization of the flow model (call it n = 0, Figure 7) and used to generate both (1) a steady state (equilibrium) temperature and flow field under fixed temperature and pressure boundary conditions described above and (2) a forward resistivity simulation. These solutions were regarded as the "truth" in which a subsequent two-stage MCMC process (based upon additional independent realizations

n ≥ 1) was initiated to match the data. In this scenario, the "measured" temperatures were those identified at the NAFEC well locations in the control (n = 0) realization, and the "measured" resistivity data were those calculated in the forward resistivity simulation in this realization. In the second case (**Scenario 2**), the actual measured NAFEC well temperatures were used in a one-stage MCMC process. Only one stage was considered in Scenario 2 because real ERT data are not available and forward codes for the MT and gravity data are still in development.

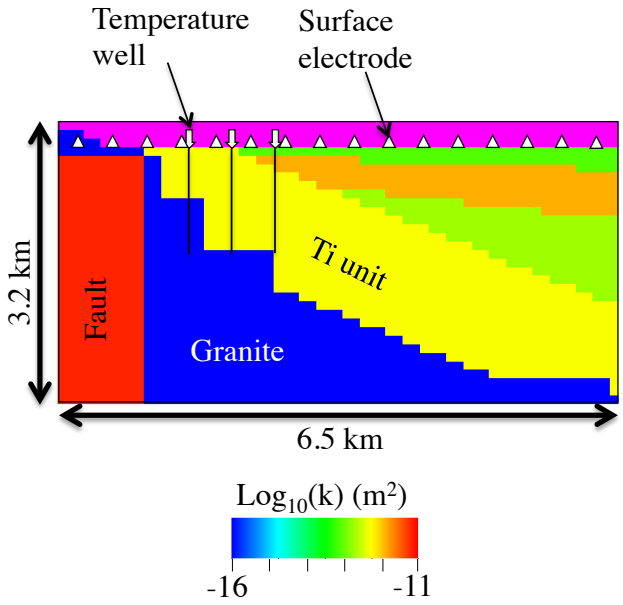

Figure 7: Two-dimensional (SW-NE) cross-section through the (n = 0) control or "true" 3D model realization used in the Scenario 1 inversion test, where color denotes permeability. Approximate positions of the NAFEC wells are shown. Note the random length and height of the CG fault (red) that can facilitate vertical hydrothermal flow from the basement to the permeable Ti Unit.

Scenario 1: In this scenario, the Monte Carlo process was distributed over two (independent) Markov Chains using 2,500 iterations each (for a total of 5000 realizations). Each realization considered the permeability of the Ti unit to be random, as well as the length, width, and permeability of the CG fault (which was of fixed width and y-axis location). Figure 8 shows example temperature fields derived from an isolated hydrothermal flow model realization and the control or "true" model realization. These are distinguished by the fact that the CG fault does (right) or does not (left) connect with the Ti Unit, thus affecting the degree to which hydrothermal flows can reach and influence temperatures in the shallower portions of the domain, near the wells. Figure 9 shows the mean permeability distributions from the top 10% of the inversion results for this scenario, as derived from Stage 1 only (upper left), Stage 2 only (upper right) and from the joint Stage 1 and Stage 2 inversion. The blurriness in the permeability values near the perimeter of the CG fault is indicative of the variability in its position in each realization. Notice how the joint inversion steers the fault position to the true value used in this example (n = 0).

Scenario 2: In this scenario, the Monte Carlo process was distributed over six (independent) Markov Chains using 5,000 iteration realizations each (for a total of 30,000 realizations). As above, each realization considered the permeability of the Ti unit to be random, as well as the length, width, and permeability of the CG fault. In addition, the CG fault was also assumed to have a random width and registration along the y-axis. Figure 10 shows the mean permeability and temperature distributions derived from the top 10% of the Scenario 2 inversion results (Stage 1 only).

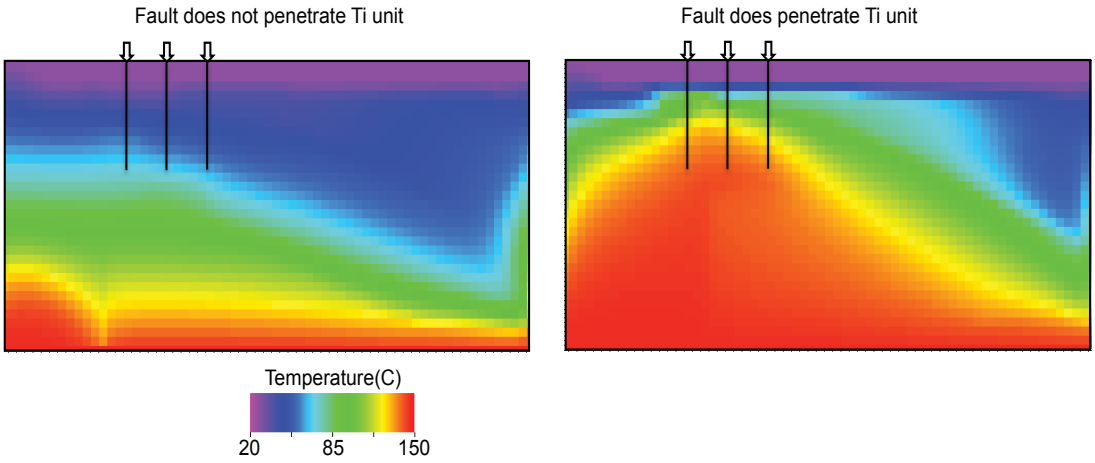

Figure 8: temperature fields derived from an isolated hydrothermal flow model realization (left) and from the control or "true" realization in the Scenario 1 inversion

Figure 11 compares the predicted data from these simulations (means and standard deviations) with the observed NAFEC well temperature profiles. Figure 12 shows the (posterior) distribution of (Ti and CG fault) permeability values present in the top 10% results compared against their original (prior) distributions from Table 1. Notably, the inversion process has significantly reduced the "uncertainty" or distributional range of the Ti permeability distribution, while that of the CG fault has not changed much at all. This is likely due to the fact that the original (prior) range of the CG fault permeability is generally high enough to facilitate flow for all values in the range – once a connection with the Ti unit is established, and that connection itself will occur or not occur as a function of the random fault dimensions. The importance of the fault connection is shown in Figure 13, where in an analog of Figure 11, very poor temperature matches are obtained when the CG fault is forcibly excluded from the analysis. This demonstrates the

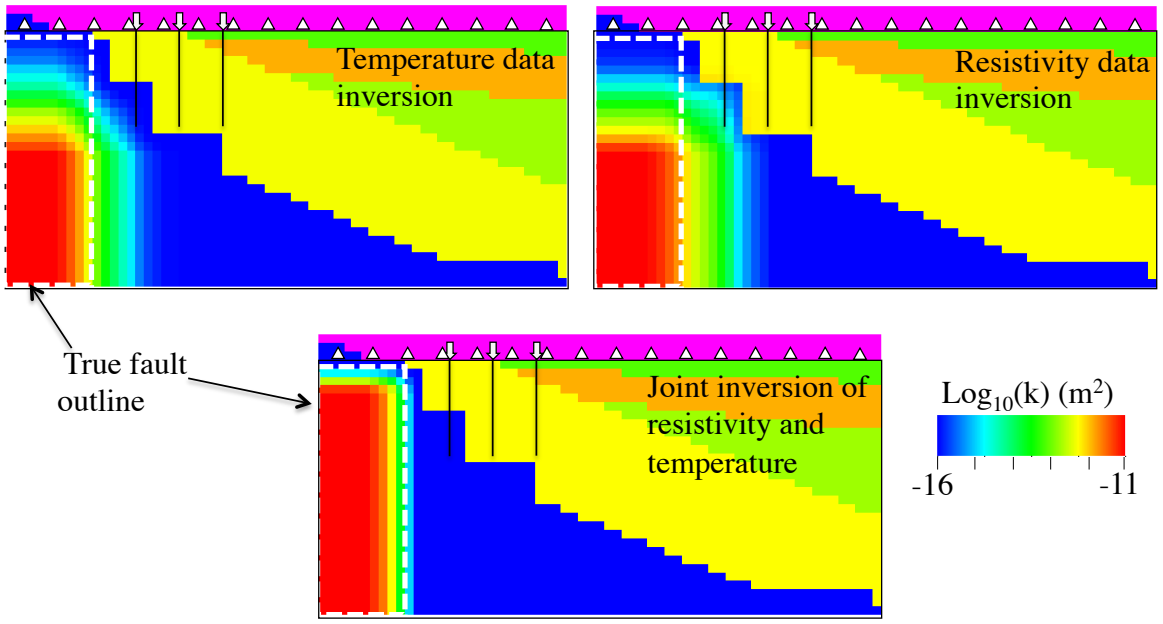

Figure 9: Mean permeability distributions from the top 10% of the inversion results in Scenario 1 derived from Stage 1 only (upper left), Stage 2 only (upper right) and from the joint Stage 1 and Stage 2 inversion (compare with control model in Figure 7)

importance of this feature and illustrates the utility of the inversion approach in terms of evaluating different geothermal model hypotheses.

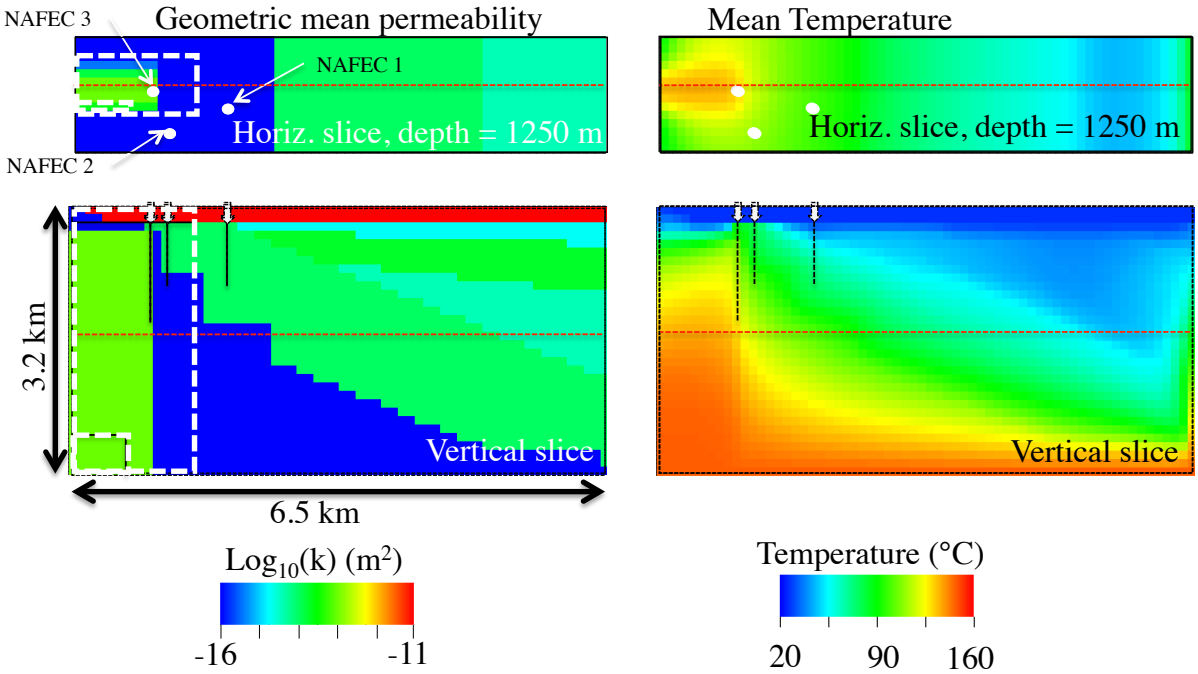

Figure 10: Mean permeability and temperature distributions derived from the top 10% of the Scenario 2 inversion results (Stage 1 only). Horizontal (top) and vertical (bottom) cross-sectional slices are shown. The dashed, white lines indicate the prior range of the uncertain CG fault length, height, and thickness (although not its y-axis position).

CONCLUSIONS AND NEXT STEPS

A stochastic inverse algorithm to jointly analyze multiple geophysical and hydrological datasets has been applied to a provisional geothermal prospect. The algorithm evaluates competing hypotheses, generates alternative models and corresponding likelihoods to estimate uncertainties associated with the alternatives. The results have illustrated how the algorithm can be used to reduce both structural and parametric uncertainty in a reference, *a-priori* model representation of the system, especially when different types of data sets are available. In the current application, the importance and influence of a small-scale fault that facilitates vertical flow of hydrothermal fluids to the sample observation wells was demonstrated. The results suggest (so far) that potential geothermal production wells would have to be carefully focused in or near this feature for a successful implementation.

In the future, the algorithm will be expanded to integrate additional magnetotellurics (MT) and surface heat flux data into the inversion process. Constraints related to the evolving computational complexity and roles of boundary condition and other operational assumptions will be examined in more detail in light of their effect on the inversion results, interpretations, and conclusions. The use of reduced-order forward models to reduce computational effort of the MCMC process will also be examined as a means to more effectively identify model sensitivities as well as guide the inversion process to a state where complex models can be better applied.

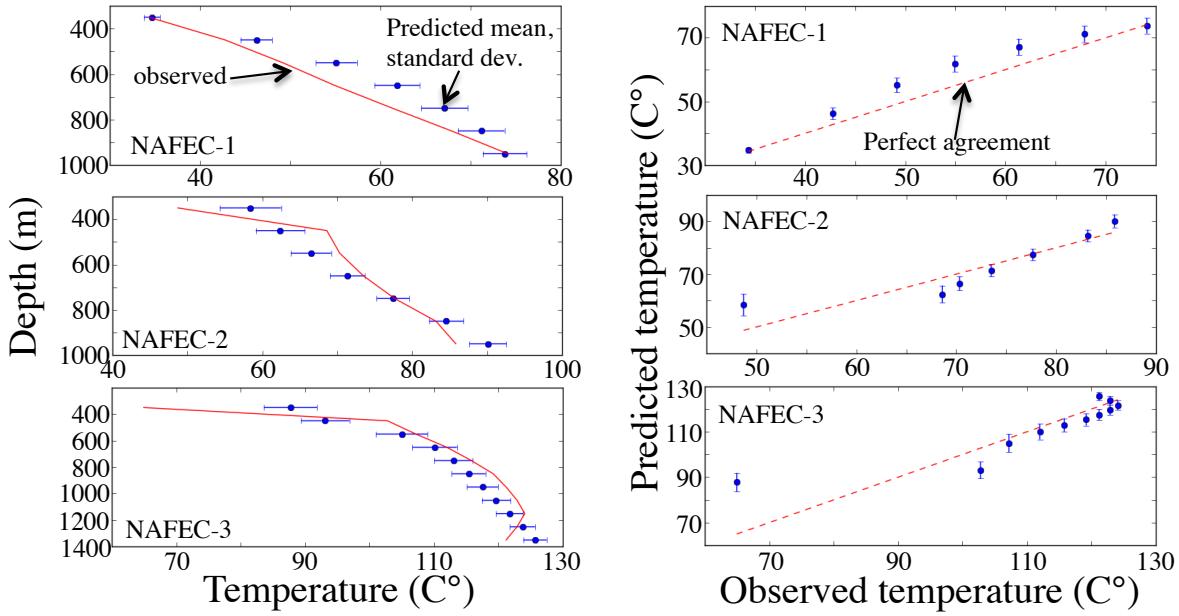

Figure 11: "Matches" of the top 10% of the Stage 1 temperature predictions at the NAFEC wells (means and standard deviations) compared with the observed profiles.

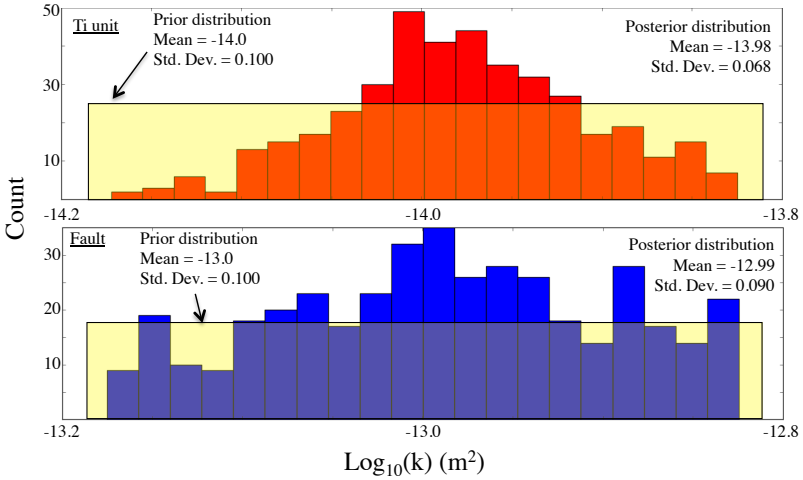

Figure 12: (Posterior) distribution of (Ti and CG fault) permeability values present in the top 10% inversion results for the Scenario 2 test, compared against their original (prior) distributions from Table 1.

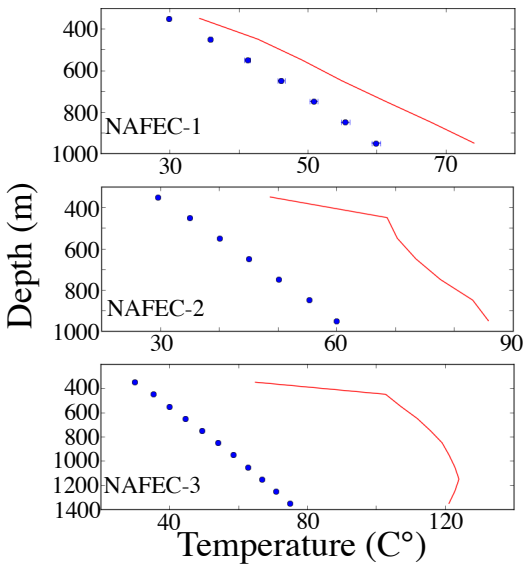

Figure 13: Temperature matches when the CG fault is forcibly excluded from the analysis (Compare with Figure 11).

Acknowledgements: This work was performed under the auspices of the U.S. Department of Energy by Lawrence Livermore National Laboratory under Contract DE-AC52-07NA27344. We appreciate the support of the DOE GTO office under award DE-EE24675. We also thank the Navy geothermal program for providing data.

REFERENCES

Bjornstad, S., B. Hall, J. Unruh, K. Richards-Dinger, (2006), "Geothermal Resource Exploration, NAF El Centro – Superstition Mountain Area, Imperial Valley, California", GRC 2006.

Chen, J., G. Hoversten, K. Key, G. Nordquist, and W. Cumming (2012), Stochastic inversion of magnetotelluric data using a sharp boundary parameterization and application to a geothermal site, Geophysics, 77(4), E265-E279

Dutcher, L. C., W. F. Hardt, and W. R. Moyle, Jr., (1972): Preliminary appraisal of ground water storage with reference to geothermal resources in the Imperial Valley area, California, Geological Survey Circular 649, prepared in cooperation with the US Bureau of Reclamation, US Geological Survey, Washington, DC.

Jardani, A., and A. Revil, 2009, Stochastic joint inversion of temperature and self-potential data, Geophys. Jour. Int., 179(1), 640-654.

LaBrecque, D. J., G. Morelli, W. Daily, A. Ramirez, and P. Lundegard, 1999, Occam's inversion of 3D electrical resistivity, in *Three-Dimensional Electromagnetics*, eds. M. Oristaglio, B Spies, and M. Cooper, pp. 575-590, Soc. Expl. Geophys., Tulsa, OK.

Loeltz, O. J., B. Irelan, J. H. Robison, and F. H. Olmsted (1975), Geohydrologic reconnaissance of the Imperial Valley, California, Geological Survey Professional paper 486 K, US Geological Survey, Washington, DC.

Metropolis, N., A. Rosenbluth, M. Rosenbluth, A. Teller, and E. Teller (1953), Equation of state calculations by fast computing machines, *J. Chem. Phys*., *1*, no. 6, 1087-1092.

Mosegaard, K., and A. Tarantola (1995), Monte Carlo sampling of solutions to inverse problems, Journal of Geophysical Research, 100, no. B7, 12431-12447.

Nitao, J.J., User's Manual for the USNT Module of the NUFT Code, Version 3.0 (NP-phase, NC-component, Thermal). Lawrence Livermore National Laboratory, UCRL-MA-130653-Rev-2 (June 1, 2000)

Nitao, J.J. Nitao, (1998), "Reference manual for the NUFT flow and transport code, Version 2.0", Technical Report UCRL-MA-130651, Lawrence Livermore National Laboratory, Livermore, CA.

Ramirez, A., W. McNab, Y. Hao, D. White, J. Johnson, 2012 (in press), Estimating reservoir permeabilities using the seismic response to CO2 injection and stochastic inversion. Int. J. Greenhouse Gas Control (2012), http://dx.doi.org/10.1016/j.ijggc.2012.11.031.

Ramirez, A. L., J.J. Nitao, W.G. Hanley, R.D. Aines, R.E. Glaser, S.K. Sengupta, K.M. Dyer, T.L. Hickling, W.D. Daily, 2005, Stochastic Inversion of Electrical Resistivity Changes Using a Markov Chain, Monte Carlo Approach, Journal of Geophysical Research, vol 110, B02101, doi:10.1029/2004JB003449, also in UCRL-JRNL-155048 Rev. 3, Lawrence Livermore National Lab., Livermore CA.

Tiedeman, A., S. Bjornstad, S. Alm, L. Frazier, D. Meade, C. Page, M. Lazaro, J. Woolford, and B. Crowder, (2011), "Intermediate Depth Drilling and Geophysical Logging Results at Superstition Mountain, Naval Air Facility El Centro, California", GRC Transactions, **35**.

Tompson, A. F. B, Z. Demir, J. Moran, D. Mason, J. Wagoner, S. Kollet, K. Mansoor, and P. McKereghan (2008), Groundwater Availability Within the Salton Sea Basin: Final Report, Lawrence Livermore National Laboratory, Livermore, CA (LLNL-TR-400426).